Available online at www.sciencedirect.com
ScienceDirect
Remote Sensing of Environment 112 (2008) 1895–1908
Remote Sensing of Environment
www.elsevier.com/locate/rse

Quantification of impervious surface in the Snohomish Water Resources Inventory Area of Western Washington from 1972–2006

Scott L. Powell [a,*], Warren B. Cohen [a], Zhiqiang Yang [b], John D. Pierce [c], Marina Alberti [d]

[a] U.S.D.A. Forest Service, Pacific Northwest Research Station, 3200 SW Jefferson Way, Corvallis, OR 97331, United States
[b] Department of Forest Science, Oregon State University, 321 Richardson Hall, Corvallis, OR 97331, United States
[c] Washington State Department of Fish and Wildlife, Natural Resources Building, 1111 Washington St. SE, Olympia, WA 98501, United States
[d] Department of Urban Design and Planning, University of Washington, Box 355740, Seattle, WA 98105, United States

Received 21 May 2007; received in revised form 20 September 2007; accepted 22 September 2007

Abstract

A 34 year time series (1972–2006) of Landsat imagery for a portion of Snohomish and King Counties, Washington (the Snohomish Water Resource Inventory Area (WRIA)) was analyzed to estimate the amount of land that was converted into impervious surface as a result of urban and residential development. Spectral unmixing was used to determine the fractional composition of vegetation, open, and shadow for each pixel. Unsupervised and supervised classification techniques were then used to derive preliminary land cover maps for each time period. Digital orthophotos were used to create agricultural, forest management, high elevation, and riparian masks. In conjunction with established Urban Growth Areas (UGAs), these masks were utilized for the application of spatial rules that identified impervious surface as a surrogate for urban and residential development. Temporal rules, that minimized classification error, were developed based on each pixel's classified trajectory over the time series of imagery. Overall cross-date classification accuracy for impervious v. non-impervious surface was 95%. The results of the analysis indicate that the area of impervious surface in the Snohomish WRIA increased by 255% over 34 years, from 3285 ha in 1972 to 11,652 ha in 2006. This approach demonstrates the unique value of the 35 year Landsat archive for monitoring impervious surface trends in rapidly urbanizing areas.

Keywords: Impervious surface; Landsat; Multitemporal; Change detection; Urban sprawl; Spectral unmixing; Washington State

1. Introduction

Land cover change is a significant concern in rapidly urbanizing areas. As land is converted into urban and residential, fundamental changes occur in the properties of ecosystems, including how water and nutrients are cycled (Tang et al., 2005) and how habitat is allocated to flora and fauna (Radeloff et al., 2005). The area around Seattle, Washington has experienced rapid land cover change in recent decades. The combined population of King County and Snohomish County increased from 1.4 million in 1970 to 2.5 million in 2005 (Washington Office of Financial Management, 2007). Despite this population growth, the extent of increase in impervious surface area due to urban and residential development during recent decades remains unquantified. We sought to quantify these changes using a time series of 13 Landsat satellite images (1972–2006) for a nearly 500,000 ha area near Seattle, Washington, known as the Snohomish Water Resource Inventory Area (WRIA).

One of the key challenges in urban remote sensing is to properly discriminate land cover classes in a heterogeneous context (Cadenasso et al., 2007). Traditional per-pixel, spectrally-based remote sensing methods have typically been limited in their applicability to urban environments (Lu & Weng, 2005), largely because land cover dynamics in urban environments often occur at the sub-pixel level. For example, a new house might occupy only a fraction of a Landsat pixel (28.5 m). While there are alternatives to moderate resolution imagery (e.g. IKONOS (Small, 2003)), no alternative offers the long term perspective (35 years) of Landsat imagery, or the practical and inexpensive coverage of such a large area. Given the benefits of Landsat imagery, the use of classification techniques that explicitly deal

* Corresponding author. Tel.: +1 541 750 7409.
E-mail address: scottpowell@fs.fed.us (S.L. Powell).

0034-4257/$ - see front matter © 2007 Elsevier Inc. All rights reserved.
doi:10.1016/j.rse.2007.09.010

with sub-pixel composition may be better suited to the issues of urban heterogeneity and scale than traditional per-pixel classifiers. Sub-pixel classification techniques enable the quantification of percent impervious surface, which is a useful surrogate for urban and residential development (Arnold & Gibbons, 1996; Lu & Weng, 2006), and includes roads, parking lots, roofs, and a variety of other non-porous surfaces. Several previous studies have used regression-tree analysis to quantify sub-pixel imperviousness in urban areas (Yang, Huang et al., 2003; Yang, Xian, et al., 2003; Xian & Crane, 2005). This approach, however, does not yield information on the non-impervious component of each pixel.

To adequately characterize urban environments, it is necessary to quantify the impervious and non-impervious components of each pixel. Ridd (1995) proposed the vegetation, impervious surface, and soil (V–I–S) model to facilitate the classification of urban areas. The V–I–S model has been widely used for spectral unmixing (Phinn et al., 2002; Wu, 2004), a technique that enables the decomposition of pixels into fractional components (or end-members). Wu and Murray (2003), and Wu (2004) compared several spectral unmixing models for estimation of impervious surface distribution in Columbus, OH, and found that the three end-member V–I–S model (including brightness normalization) was the most effective. Other studies, however, have demonstrated the effectiveness of a variety of different end-member combinations, such as high-albedo, low-albedo, and vegetation (Small, 2002), the inclusion of shade as an end-member (Alberti et al., 2004; Lu & Weng, 2004), and allowance for variable numbers and types of end-members (Dennison & Roberts, 2003; Rashed et al., 2003). Lu and Weng (2004) demonstrated that green vegetation, shade, and soil or impervious surface were the most effective end-members for spectral unmixing in Indianapolis, IN. Selection of these three end-members explicitly acknowledges that impervious surfaces are spectrally similar to bare soil, sand, or rock, and may be inseparable (Guindon et al., 2004; Lu & Weng, 2004; Ridd, 1995; Wu & Murray, 2003). Therefore in addition to spectral information, the spatial and temporal information derived from pixels are equally important for accurate discrimination of impervious surface.

Land cover classification is aided by consideration of landscape, or spatial context. For example, consider a pixel containing no vegetation. Spectrally-based remote sensing methods can accurately identify the lack of vegetation, but cannot accurately resolve whether the pixel is man-made impervious surface or bare soil. However, if this pixel is located within an urban setting, we can assume with some confidence that the land cover is impervious surface. Conversely, if this pixel is identified on a high mountain ridge, we can assume with some confidence that the land cover is bare soil or rock. In this manner, spatial context has been previously incorporated to improve land cover classifications. Yuan et al. (2005) relied on post-classification refinements, including the use of spatial masks and manual digitizing from digital orthophotos, to minimize classification error. Likewise, Yang (2002) used spatial reclassification procedures, including image smoothing and manual digitizing to reduce land cover confusion. Such contextual reclassification techniques (Gong & Howard, 1992) draw upon the expert-knowledge of the analysts, and enable logical stratification and masking of the study area.

The inclusion of spatial context is a significant improvement, but it may not go far enough. Another key factor for classifying land cover is temporal context. The temporal trajectory of a pixel through a time series of imagery can yield important clues about land cover that single images cannot (Liu & Zhou, 2004). For example, consider an annual time series of land cover classifications, and a pixel changing back and forth between vegetated and non-vegetated classes through the time series. We can assume with some confidence, in this case, that vegetation management or phenology are driving the spectral response of this pixel. Then, considering the spatial context, farmland for example, we can assume with confidence that the land cover is cropland. Conversely, consider a pixel classified as non-vegetated through the entire time series. Then, considering the spatial context, within a city for example, we can assume with some confidence that the land cover is impervious surface.

Incorporating spectral, spatial, and temporal contexts should enable more accurate quantification of change in impervious surface than relying on one or two contexts only. This paper presents methods for quantifying change in impervious surface over 34 years in the Snohomish WRIA, using all three contexts. We approached the study in three key stages:

1. Acknowledging the spatial resolution of Landsat imagery, we employed a spectral unmixing technique for determining sub-pixel land cover composition.
2. Recognizing the spectral overlap between impervious surface and soils, we combined spectral-based classification with spatial knowledge-based classification to identify impervious surface associated with urban and residential development.
3. Leveraging the temporal information from the 34 year Landsat time series, we devised a set of temporal rules to reduce classification error.

2. Methods

The Snohomish WRIA is a complex mixture of forest, agriculture, residential, and urban components. The focus of this research was primarily to characterize change in the urban and residential components, resulting from densification of existing urban and residential areas, as well as from conversion of forest and agricultural land. To simplify the analysis, we stratified the WRIA with spatial masks where expected land-use activities either excluded or permitted urban and residential development. Urban Growth Areas (UGAs), delineated by Snohomish and King Counties, contain the core urban areas, while outside of these, lower-density residential development is permitted. However, much of study area outside of UGAs consists of agricultural lands, riparian areas, forest management, high-elevation mountainous areas, water, snow, and ice, and is largely inaccessible to urban and residential development.

To map urban and residential growth over 34 years in the Snohomish WRIA, we used spectral unmixing to discriminate sub-pixel fractional land cover composition for each of the 13

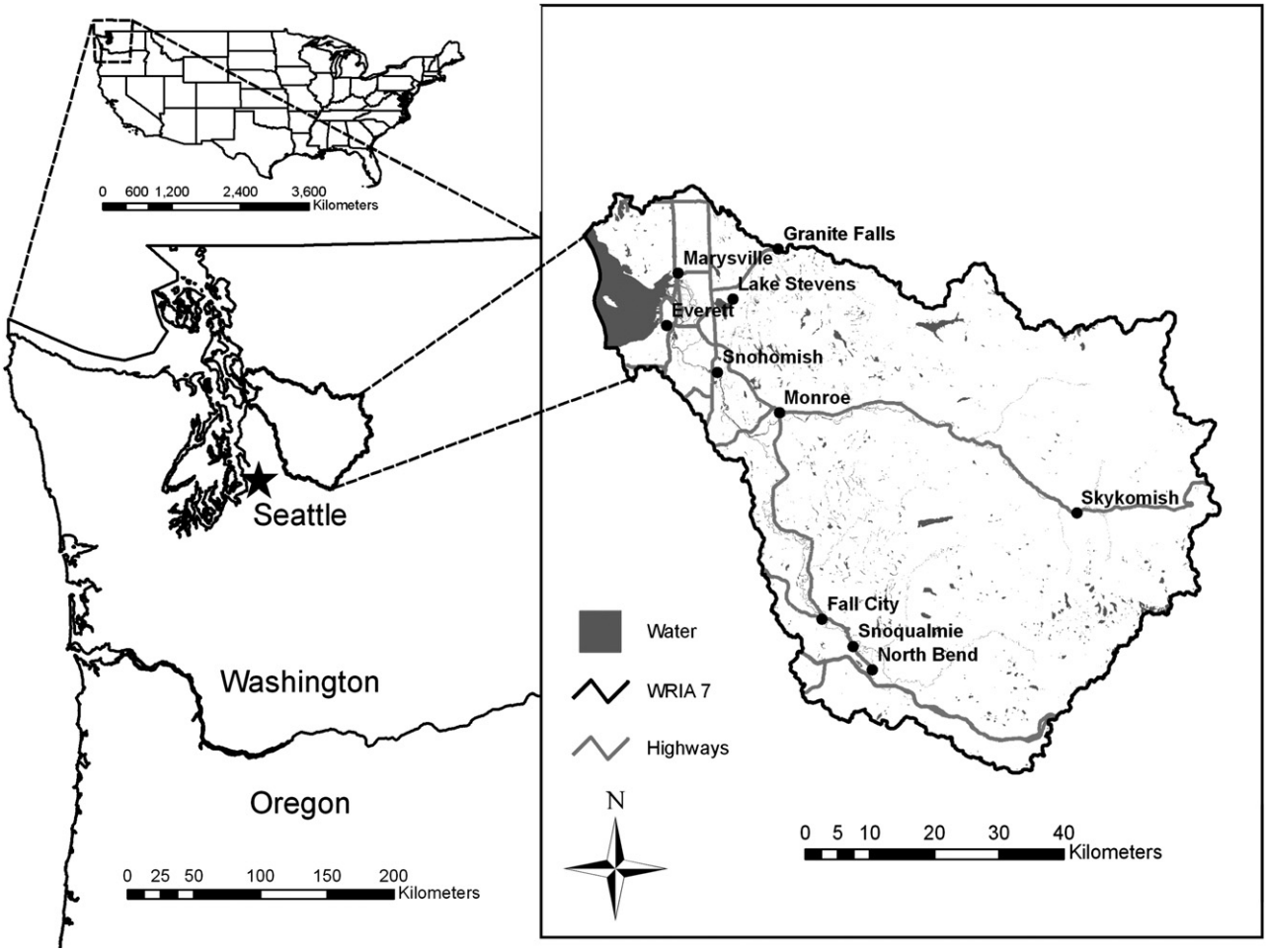

Fig. 1. Snohomish WRIA 7 study area in relation to the conterminous U.S., and Seattle, Washington. Major towns, highways, and water bodies within WRIA 7 are shown in the inset.

dates of Landsat imagery. Then we used both unsupervised and supervised classification to convert the fractional composition maps into preliminary land cover maps for each date. Based on spatial context from the stratification and masking, we identified impervious surface associated with urban and residential development. Finally, to minimize classification error, we developed a technique that identified misclassified pixels by leveraging the temporal signal from the Landsat time series.

2.1. Study site

The state of Washington is divided into 62 WRIAs. The study area is a 494,839 ha region northeast of Seattle, WA, delineated as the Snohomish WRIA (Fig. 1). The WRIA encompasses the Snoqualmie and Skykomish watersheds, and their convergence forming the Snohomish River and its outlet into the Puget Sound at Everett, WA. Elevations within the study area range from sea level along the Puget Sound to 2408 m in the Cascade Mountains along the eastern portions of the WRIA. Urban and residential areas are concentrated in the lower elevations, primarily near Everett, WA, and along the valley bottoms following the Snohomish, Snoqualmie, and Skykomish rivers. Vegetation in the study area ranges from agriculture and pasture in the lower elevations, to broadleaf-dominated forests in the middle elevations, and needleleaf-dominated forests in the higher elevations. The highest elevations in the study area consist of alpine tundra, rock, and persistent snow and ice fields.

2.2. Preprocessing

We acquired 13 late-summer Landsat satellite images of the study area, spanning 34 years (Table 1). The TM and ETM+ images were either acquired with 28.5 m pixel resolution or resampled to 28.5 m. The MSS images were acquired with 57 m pixel resolution and resampled to 28.5 m to match the TM and ETM+ resolution. The 1975 (MSS) and 2000 (ETM+) images were acquired orthorectified, and used as reference images for geometric co-registration and orthorectification using an automated tie-point program (Kennedy & Cohen, 2003). All 13 images were co-registered to the UTM (WGS84) coordinate system with root mean square errors less than 0.5 pixels per image.

The Landsat image time series was then radiometrically normalized. The year 2000 ETM+ image was acquired in

Table 1
Date, WRS path/row, and sensor type for each of the 13 Landsat satellite images used in the study

Date	WRS path/row	Sensor
07/29/1972	WRS1 50/27	Landsat 1 MSS
07/23/1975	WRS1 50/27	Landsat 2 MSS
08/03/1978	WRS1 50/27	Landsat 3 MSS
08/23/1981	WRS1 50/27	Landsat 3 MSS
08/23/1985	WRS2 46/27	Landsat 5 TM
08/31/1988	WRS2 46/27	Landsat 5 TM
09/22/1990	WRS2 46/27	Landsat 5 TM
08/29/1993	WRS2 46/27	Landsat 5 TM
08/21/1996	WRS2 46/27	Landsat 5 TM
08/27/1998	WRS2 46/27	Landsat 5 TM
09/25/2000	WRS2 46/27	Landsat 7 ETM+
08/14/2002	WRS2 46/27	Landsat 7 ETM+
09/02/2006	WRS2 46/27	Landsat 5 TM

calibrated surface reflectance from the Landsat Ecosystem Disturbance Adaptive Processing System (LEDAPS) (Masek et al., 2006). We used this surface reflectance image as reference for the Multivariate Alteration and Detection (MAD) relative radiometric normalization procedure (Canty et al., 2004). Using band-wise regression of the six reflective bands, each of the other eight TM and ETM+ target images were converted to surface reflectance and matched to that common radiometric scale (Schroeder et al., 2006). Subsequent to normalization, the ETM+ and TM image were converted to Thematic Mapper Tasseled Cap brightness, greenness, and wetness using the coefficients for reflectance factor data (Crist, 1985). To normalize the MSS imagery with respect to ETM+ and TM, we used the vegetation indices brightness and greenness (wetness can't be derived from MSS) with MAD rather than the reflectance bands, using the original coefficients for MSS Tasseled Cap brightness and greenness (Kauth & Thomas, 1976). Brightness and greenness derived from the year 2000 ETM+ surface reflectance image were used as reference for MAD.

2.3. Spectral unmixing

Spectral unmixing was used to extract sub-pixel fractional composition. Since urban and residential dynamics can be heterogeneous and fine grained, we wanted to use a technique that could quantify the vegetated and non-vegetated fractions of each pixel. Linear spectral unmixing presumes that a pixel's reflectance is a linear combination of a set number of spectral end-members (Small, 2002). To identify these spectral end-members, we plotted the two-dimensional distributions of Tasseled Cap brightness v. greenness, from which end-members were delineated by co-located examination of imagery and digital orthophotos. We chose brightness v. greenness plots for end-member selection for two reasons. First, brightness v. greenness plots are directly interpretable in terms of relative vegetation and soil amounts (Crist & Cicone, 1984). Second, as demonstrated in the description of radiometric normalization, brightness and greenness are a practical bridge between MSS and TM/ETM+ imagery. Negative greenness values, i.e., values below the "soil line", were not included in the plots as they represented completely non-vegetated areas and confounded the interpretation of spectral end-members. Moreover, we assumed with high certainty that pixels located below the soil line would later "unmix" as 100% non-vegetated (Crist & Cicone, 1984).

Using the 2006 Landsat TM image, we identified three spectral end-members representing 1) sunlit soil, rock, or impervious surface (100% open), 2) green vegetation (100% vegetation), and 3) shadow or water (100% shadow or water) (Fig. 2). Given radiometric normalization of the full Landsat time series, we used the 2006 end-member signatures to unmix the raw TM and ETM+ imagery (bands 1–5, 7) to derive the pixel-level proportions of the three end-members for each of the nine TM/ETM+ images. Then, using the 1981 Landsat MSS image, we identified the same three spectral end-members. We used these signatures to unmix the raw MSS imagery (i.e., bands) to derive the pixel-level proportions of the three end-members for each of the four MSS images. It was necessary to unmix the raw bands, as opposed to the Tasseled Cap bands, to have adequate spectral dimensionality for unmixing three end-members. The result of the spectral unmixing was a map for each of the 13 time periods depicting the relative percentages of open, vegetation, and shadow (or water) for each pixel.

2.4. Preliminary classification

A first classification was derived to group the fractional end-member proportions into preliminary land cover classes, resulting in preliminary maps for each time period. For this we used unsupervised classification to identify a training data set, and then performed supervised classification on each year of imagery using these training data. This preliminary classification served to separate pixels along a continuum of vegetation amount from fully vegetated to open. The open amount represented either impervious surface, bare soil, or rock, depending upon spatial and temporal context.

Using the 2006 end-member proportions, we performed an ISODATA unsupervised classification (Jensen, 1996). Through visual examination of Landsat imagery and digital orthophotos,

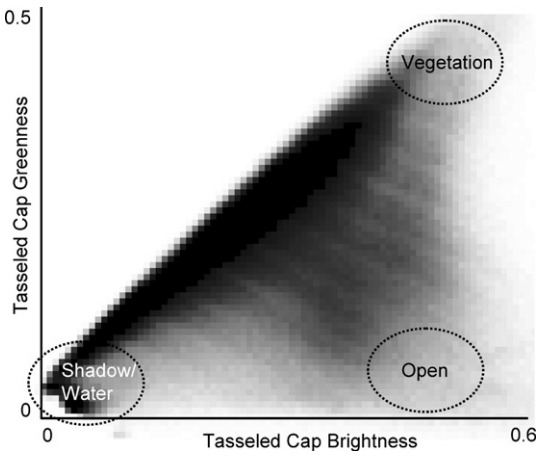

Fig. 2. Spectral end-members in Tasseled Cap brightness v. greenness space.

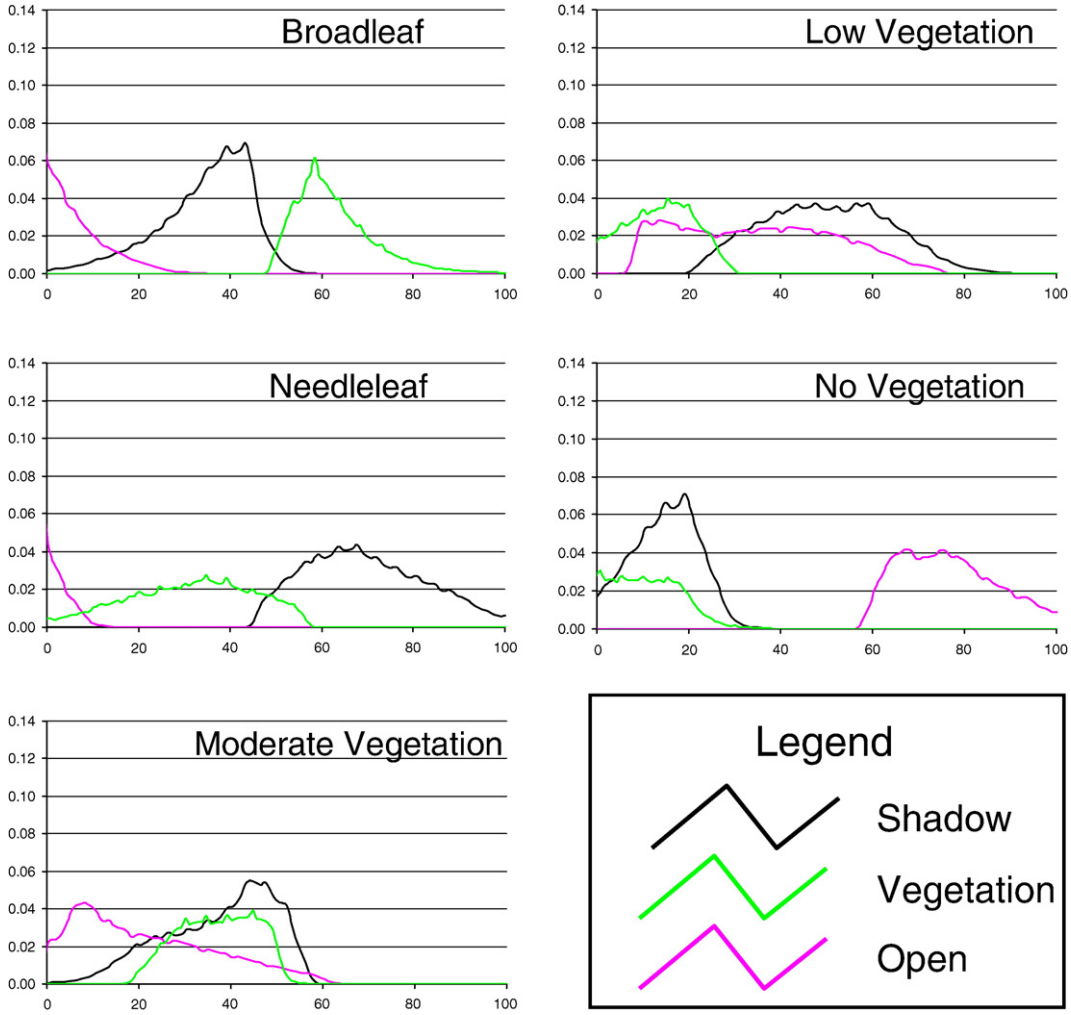

Fig. 3. End-member frequency distributions for each of the land cover classes derived from unsupervised classification. *X*-axes are the end-member fractional composition; *Y*-axes are the frequencies.

we interpreted and reclassified the 50-class output from the unsupervised classification into five classes ranked from high to no vegetation amount:

1) high vegetation: broadleaf-dominated
2) high vegetation: needleleaf-dominated
3) moderate vegetation
4) low vegetation
5) no vegetation

Class one represented high vegetation amount dominated by broadleaf plants (predominantly forest vegetation) containing low open, moderate shadow, and high vegetation end-member proportions (Fig. 3). Some pixels in this class contained green agricultural vegetation, which was not always spectrally distinct from broadleaf-dominated forest. Class two represented high vegetation amount, dominated by needleleaf forest. This class consisted of low open, moderate vegetation, and high shadow end-member proportions. Classes three through five contained fractions of open and vegetation components in order of increasing open amount and generally decreasing vegetation amount. Class three, moderate vegetation, contained moderate vegetation and shadow proportions, but low open proportion. Class four, low vegetation, contained lower vegetation proportion, but higher open proportion. Class five, no vegetation, contained a combination of lowest vegetation and highest open proportions relative to any other class. As expected, the negative greenness pixels that were excluded from end-member selection were virtually all contained in the no vegetation class.

Using these five land cover classes identified on the 2006 image, we incorporated all of the pixels from each class into a training data set. We then applied this comprehensive training data set to a maximum likelihood supervised classification on the fractional end-member images for each Landsat date. The result was a preliminary land cover map for each of the 13 dates of Landsat imagery.

2.5. Knowledge-based classification

The preliminary land cover maps represented the extent to which spectrally-based methods alone could accurately discriminate land cover. To achieve our final objective of quantifying changes in impervious surface associated with urban and residential development, we incorporated spatial and temporal

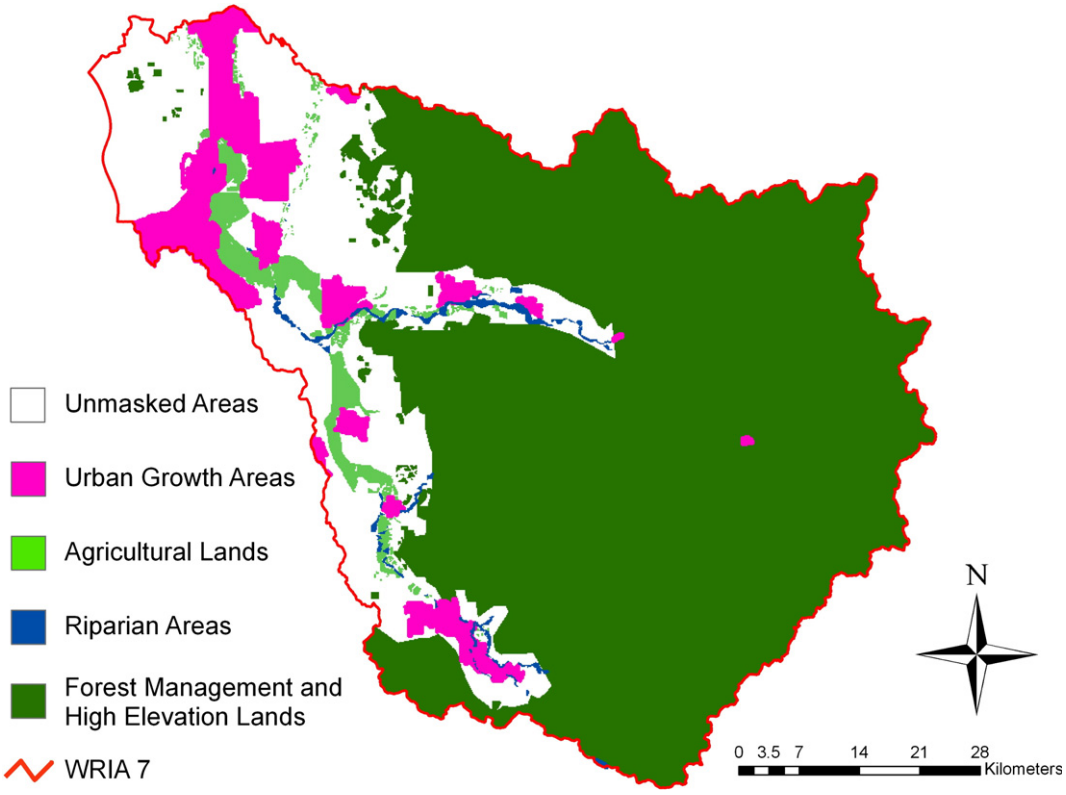

Fig. 4. Stratification masks within the study area for spatial and temporal rule application.

context into the analysis. We devised a set of knowledge-based rules for further resolving land cover classes. To implement these rules, we delineated five distinct land cover types within the study area to which different spatial and temporal rules were applied for classification purposes (Fig. 4).

1) Urban Growth Areas (UGAs) containing the urbanized cities and towns in the study area, and delineated with Snohomish County (Snohomish County Cartography/GIS Services Team, 2007) and King County (King County GIS Center, 2007) UGA polygon layers.
2) Agricultural lands containing no impervious surface. These were delineated by manual on-screen digitizing using 2005 digital orthophotos as a reference.
3) Riparian areas within or directly adjacent to major river systems, containing no impervious surface. These were delineated by manual on-screen digitizing using 2005 digital orthophotos as a reference.
4) Forest management lands with evidence of recent or on-going forest management activities, and high-elevation mountainous areas (mostly public lands) containing no impervious surface. These were delineated by manual on-screen digitizing using 2005 digital orthophotos as a reference.
5) Unmasked areas containing the remainder of the study area.

In using the 2005 digital orthophotos for digitizing the masks, we assumed that if impervious surface was absent in 2005, it was absent in all previous dates (in only the rarest circumstances would impervious surface revert back to agriculture, etc…). The masks, therefore, were not intended for analysis of the land cover that was converted to impervious during the study period.

2.5.1. Spatial rules

We carefully examined the open component of each land cover class using digital orthophotos. Both the low vegetation and the no vegetation classes contained a mixture of open components, including impervious surface, bare soil, and rock. We devised two spatial rules, to be applied independently to each date in the time series, for subdividing the low vegetation and no vegetation classes into impervious and non-impervious classes.

2.5.1.1. Rule #1. Within the UGAs, we found little soil or rock, and that the open component of low vegetation and no vegetation was almost exclusively associated with impervious surface. Therefore, within the UGAs, we reclassified no vegetation as high impervious and low vegetation as low impervious.

2.5.1.2. Rule #2. In the unmasked areas, we found that the open component of the low vegetation class was overwhelmingly associated with partially impervious surface. Therefore, in the unmasked areas, we reclassified low vegetation as low impervious.

2.5.2. Temporal rules

As the spatial rules were applied independently to each image in the time series, their application resulted in some incongruous pixel-level temporal trajectories of class labels that could be largely rectified with simple temporal rules. We analyzed the

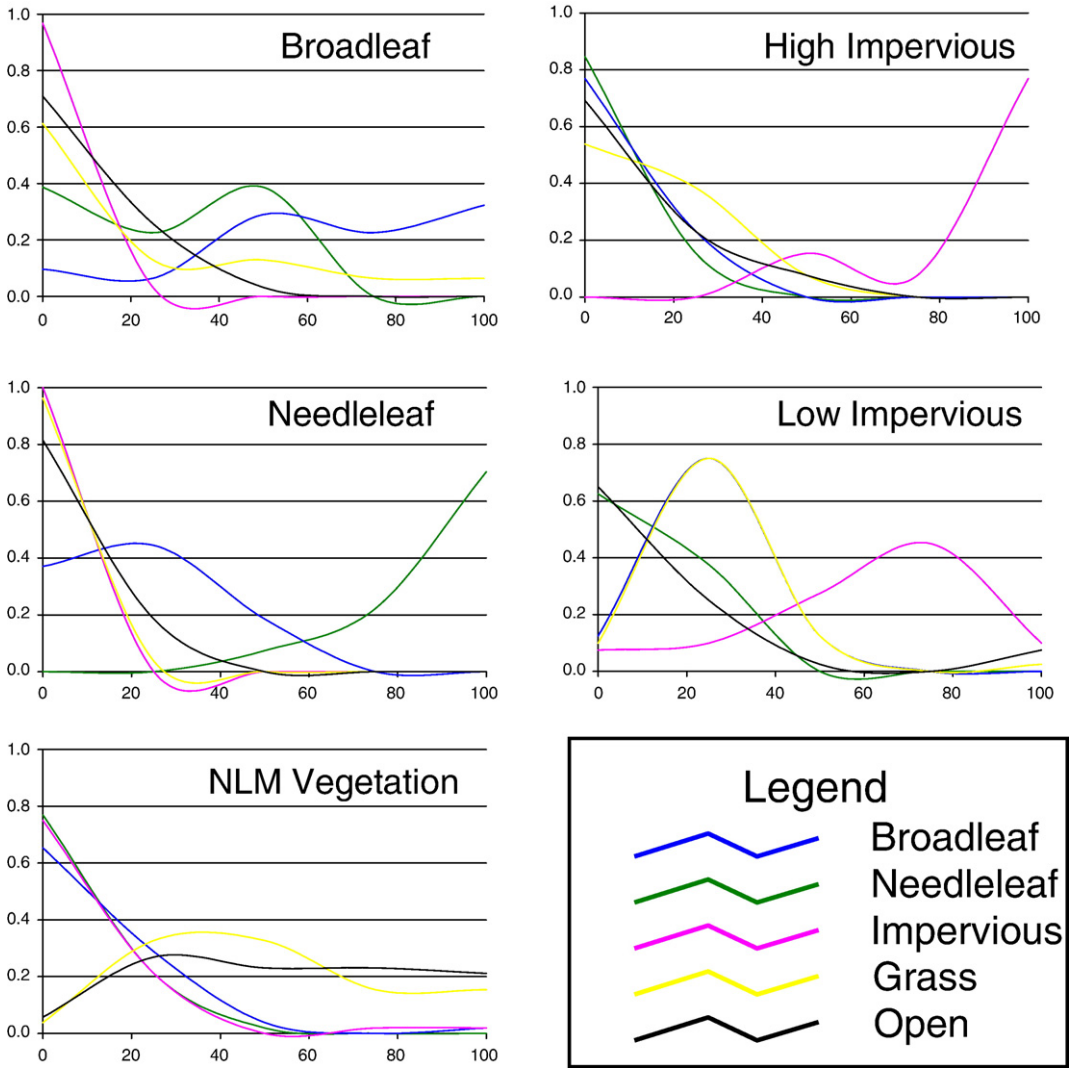

Fig. 5. Validation component frequency distributions for each of the final land cover classes, derived from aerial photo interpretation. *X*-axes are the component fractional composition; *Y*-axes are the relative frequencies.

classified trajectory of each pixel over the 13-date Landsat time series and devised two temporal rules. In doing so, we acknowledged that some errors were more tolerable than others. Consequently, we attempted to minimize the most egregious errors by flagging only those pixels that exhibited overwhelming evidence of misclassification.

2.5.2.1. Rule #3. Pixels exhibiting frequent (more than three directional-changes in impervious amount) or unlikely changes (decreases of more than one class of impervious amount) over the Landsat time series were assumed to be associated with vegetation management or phenology, and therefore not likely to be impervious surface. We reclassified these pixels from high impervious back to no vegetation, and low impervious back to low vegetation.

2.5.2.2. Rule #4. All remaining impervious pixels were then subjected to a non-reversal rule. Once a pixel became impervious, it could not revert to less-impervious or non-impervious through the remainder of the Landsat time series.

We then made a modification to the classification scheme to improve the interpretability of the final maps. Since we were primarily interested in mapping change in impervious surface, we merged no vegetation, low vegetation, and moderate vegetation into a single class, called NLM (No, Low, and Moderate vegetation). There was significant end-member overlap among these three classes, and merging them did not decrease the overall value of the final map products. Collectively, this single merged class then represented all bare soil to semi-vegetated areas, including primarily agricultural fields, clear-cuts, pastures, rock, and alpine tundra.

To finalize each of the maps, we applied three additional masks to each year of imagery: 1) a water body mask containing all ocean, lakes, and major rivers (Washington State Department of Natural Resources, 2007); 2) a road mask containing all major highways (Washington State Department of Transportation, 2007); and 3) a snow and ice mask containing all persistent glacial ice and snowfields. The road mask was incorporated directly into the high impervious class. The snow and ice mask was derived from an unsupervised classification of the Landsat

Table 2
Five-class, cross-date accuracy assessment

		Observed class						
		Broadleaf	Needleleaf	High impervious	Low impervious	NLM	Row total	Commission error
Predicted class	Broadleaf	**30**	9	0	3	1	43	0.30
	Needleleaf	2	**48**	0	2	2	54	0.11
	High impervious	0	0	**8**	5	1	14	0.43
	Low impervious	0	0	1	**24**	0	25	0.04
	NLM	20	0	1	5	**57**	83	0.31
	Column total	52	57	10	39	61	**219**	
	Omission error	0.42	0.16	0.20	0.38	0.07		
Overall accuracy = 76%; K_{hat} = 69%								

Bold numbers signify the agreement between observed and predicted classes.

image containing the maximum summer snow and ice extent (2002). With these masks, we arrived at the final land cover classification scheme:

1) water
2) high vegetation: broadleaf-dominated
3) high vegetation: needleleaf-dominated
4) no, low, and moderate vegetation (NLM)
5) low impervious
6) high impervious
7) snow and ice

2.6. Calculation of impervious surface area

To estimate the area of impervious surface in each time period, we weighted the low impervious and high impervious pixels by their sub-pixel fraction of open, from the end-member maps. This yielded a per-pixel estimate of impervious surface area for each date in the time series. To offset year-to-year variation in end-member composition (due largely to phenology), we used a three-year moving average of total impervious surface area. These final estimates yielded the 34 year trajectory of total impervious surface area across the Snohomish WRIA.

2.7. Map accuracy assessment

To validate the final maps, we devised a method to quantify the fractional composition of five interpretable land cover components from aerial photo interpretation. These land cover components – conifer forest, broadleaf forest, grass, open, and impervious – were a quantifiable bridge to the final land cover classification. We derived a class-defining reference data set from the 2006 map by sampling 163 plots, 3 × 3 pixels in size, located in homogeneous areas (all nine pixels of the same class). We stratified the sample by the proportional area of each class within the study area. For each plot, we interpreted the fractional composition of the five land cover components from year 2005 digital orthophotos. We plotted the frequency distributions of the five land cover components for each of the final land cover classes (Fig. 5). The high vegetation: broadleaf-dominated class contained high broadleaf, moderate needleleaf, and low remaining component amounts. The high vegetation: needleleaf dominated class contained high needleleaf, moderate broadleaf, and low remaining component amounts. The NLM vegetation class contained high grass and open proportions, and low other component amounts. The high impervious class contained high impervious and low other component amounts. The low impervious class contained high impervious, moderate grass and open, and low other component proportions. With these reference data, we performed a discriminant function analysis to derive a function with which to predict class membership for independent validation data.

We then derived an independent validation data set using 214 plots across six dates (1985, 1990, 1998, 2000, 2002, and 2006). We selected these dates because they corresponded to the dates of digital orthophotos and hardcopy aerial photographs that we had obtained. For each of the six image dates (out of 13), we collected approximately 35 sample plots, 3 × 3 pixels in size, located in purely homogeneous areas, stratified by the proportional area of each class within the spatial overlap of the photos and the map. For each plot, we interpreted the fractional composition of the five land cover components (conifer forest, broadleaf forest, grass, open, and impervious) from the corresponding photo. Then, using the discriminant functions derived from the class-defining reference data, we predicted the class membership for each independent validation plot. We then compared observed class membership to predicted class membership and derived traditional measures of accuracy including omission error, commission error, overall accuracy, and the Kappa statistic.

3. Results and discussion

3.1. Spatial and temporal rules

The inclusion of both spatial and temporal rules in addition to the spectral classification enabled subdivision of the low and no vegetation classes into impervious and non-impervious classes. To illustrate the effects of the spatial and temporal rules, we present the results for the 2006 map. Spatial Rule #1 resulted in 21% of the no vegetation pixels being reclassified as high impervious inside the UGAs, and 23% of the low vegetation pixels being reclassified as low impervious inside the UGAs. Outside the UGAs, spatial Rule #2 resulted in a 57% increase in the number of pixels of low impervious. To mitigate errors associated with the spatial rules, we implemented the temporal

Table 3
Two-class, cross-date accuracy assessment

		Observed class			
		Impervious	Non-impervious	Row total	Commission error
Predicted Class	Impervious	**38**	1	39	0.03
	Non-impervious	11	**169**	180	0.06
	Column total	49	170	**219**	
	Omission error	0.22	0.01		

Overall accuracy = 95%; K_{hat} = 83%

Bold numbers signify the agreement between observed and predicted classes.

rules. Temporal Rule #3 resulted in a 14% decline in the number of impervious pixels across the study area.

3.2. Map accuracy assessment

Classification error assessment, facilitated by use of multiple dates of digital orthophotos, was revealing (Table 2). Error rates were generally low for most of the five main map classes (excluding water and snow and ice, which were not assessed). The highest commission error rate was for high impervious (0.43), but this was largely balanced by the omission error rate of the same class (0.20) and that of the low impervious (0.38), which was mapped over a significantly large proportion of the map at each date. Moreover, most of the commission error associated with high impervious was the result of misclassification to low impervious. The commission error rate for low impervious was very low (0.04), and all of it was the result of misclassification to high impervious. The high omission error rate for low impervious was indicative of the significant vegetation composition of that class. Overall cross-date accuracy for the five classes was 76% (Table 2).

Although errors in each class were important, they were not equally important. For the purposes of this study, distinction among the non-impervious classes was not particularly meaningful. Focusing on the primary distinction of importance, reclassification of the final maps into two broad classes, pixels containing impervious surface and those not containing impervious surface, yielded a cross-date overall accuracy of 95% (Table 3). The higher omission error rate (0.22) v. commission error rate (0.03) for impervious was partially mitigated by the fact that nearly all of the omission error was from low impervious while all of the commission error was from high impervious.

3.3. Land cover change between 1972 and 2006

We calculated the area of impervious surface for each date by weighting the pixels of the two impervious surface classes by their open end-member proportion from mixture modeling. We found that between 1972 and 2006, the area of impervious surface increased from 3285 ha to 11,652 ha across the study area (Fig. 6), representing an increase of 255%. During that same time period, population in the two counties containing our study area (King and Snohomish) increased from 1.4 to 2.5 million, an increase of 79% (Washington Office of Financial Management, 2007). This differential growth rate between impervious surface and population is typical of urban sprawl, which has been defined as "a pattern of land-use/land-cover conversion in which the growth rate of urbanized land significantly exceeds the rate of population growth over a specified time period, with a dominance of low-density impervious surfaces" (Barnes et al., 2007). This is also supported by our observation that the low impervious class increased by over 6000 ha (2748 ha to 8946 ha) over the 34 years of this study, whereas the area classified as high impervious increased by only approximately 2000 ha (from 537 ha to 2706 ha) (Fig. 7). Moreover, we see that the low impervious increase occurred more outside of UGAs than within (Fig. 8).

In 1990, the Washington state legislature adopted the Growth Management Act, with which it attempted to concentrate urban

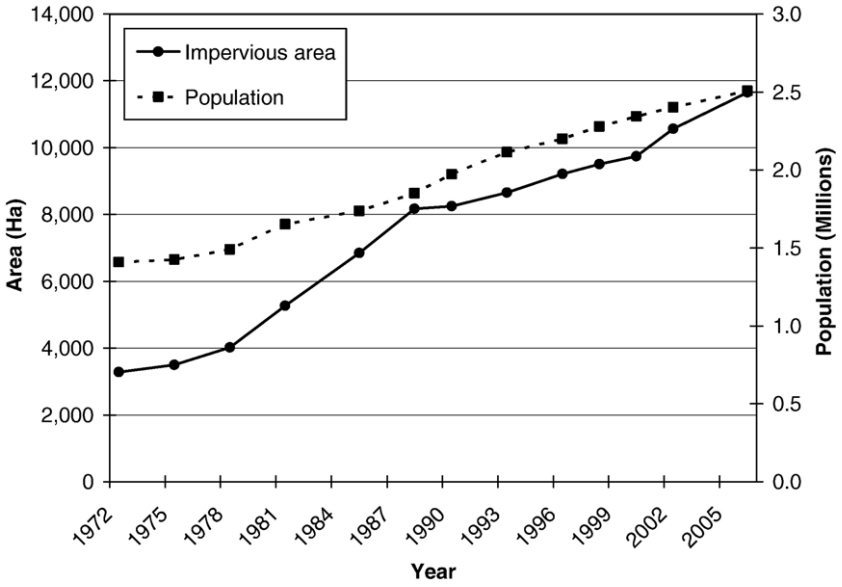

Fig. 6. Change in impervious area in the Snohomish WRIA and change in population in Snohomish and King Counties between 1972 and 2006.

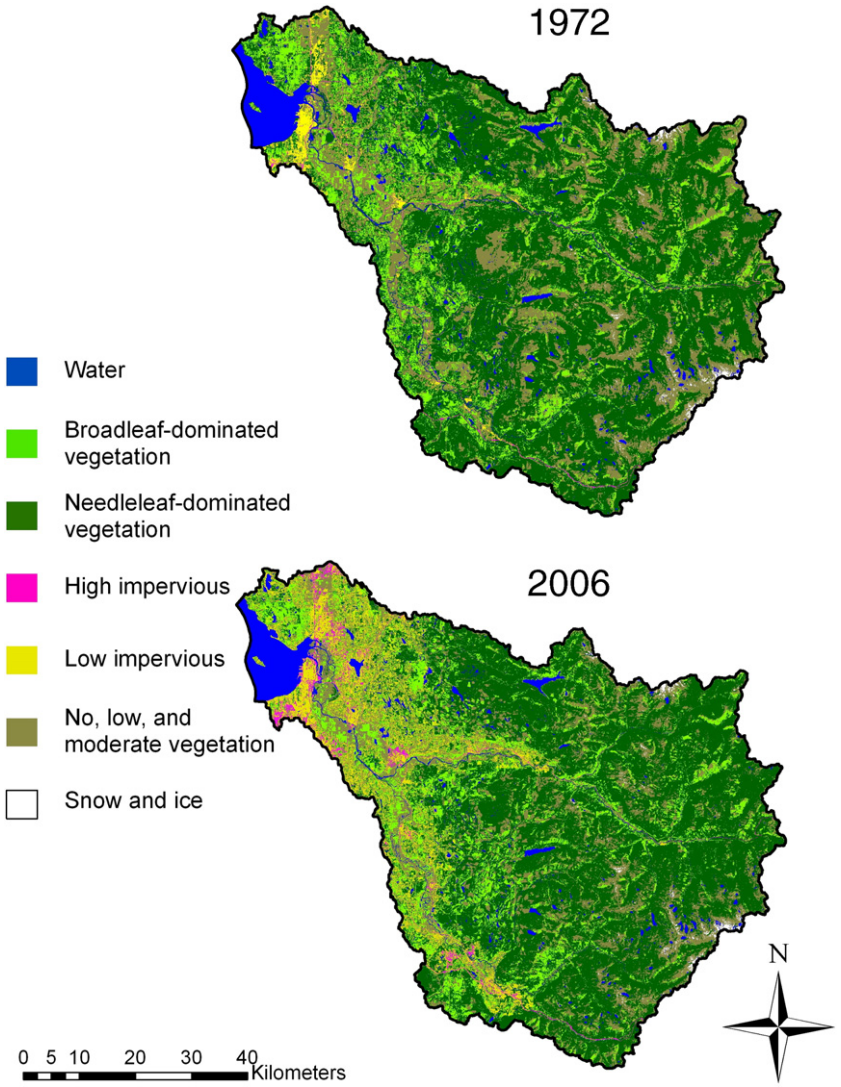

Fig. 7. Land cover and land use in the Snohomish WRIA 1972 and 2006.

development within UGAs. Based on the previous discussion that urban sprawl has a greater effect than urban densification on impervious surface growth, it appears from Fig. 6 that the rate of urban sprawl declined during the 1990's. However, the extent to which this trend is associated with the Growth Management Act cannot be fully determined by this study. Further analyses of trends in impervious surface in conjunction with social, political, and economic studies could shed light on the effect of growth management policies.

3.4. Comparison to other studies

There have been other attempts to quantify the extent of impervious surface and change through time, across the Snohomish WRIA. Although it is difficult to directly compare studies with different objectives and methods, they do serve as indirect comparisons against our results. The circa 2000 National Land Cover Data (NLCD) base (United States Environmental Protection Agency, 2007), developed through the Multiresolution Land Characteristics Consortium (MRLC), mapped impervious surface across the Snohomish WRIA (Homer et al., 2002). The 2001 NLCD map of impervious surface estimated 11,893 ha of impervious surface in the Snohomish WRIA. This is close to our 2002 estimation of 10,568 ha of impervious surface in the Snohomish WRIA. One striking visual difference between our map and the NLCD map is that the NLCD map included the full network of roads throughout the study area, many of which are most likely dirt or gravel roads. If we were to include this same network of roads (we used only major highways) in our calculation of impervious surface area, our estimate would increase to 11,936 ha. Since our overall objective, however, was to quantify the change in impervious surface between 1972 and 2006, it was not practical to incorporate these roads, since we could not verify how they have changed over time. Therefore, to estimate change in impervious surface, we relied on changes in surface reflectance, modified by spatial and temporal rules.

Another difference between our map and the NLCD map is that our map depicted substantially more spatial heterogeneity of impervious surface within urban areas, which appears to be more accurate when contrasted against digital orthophotos

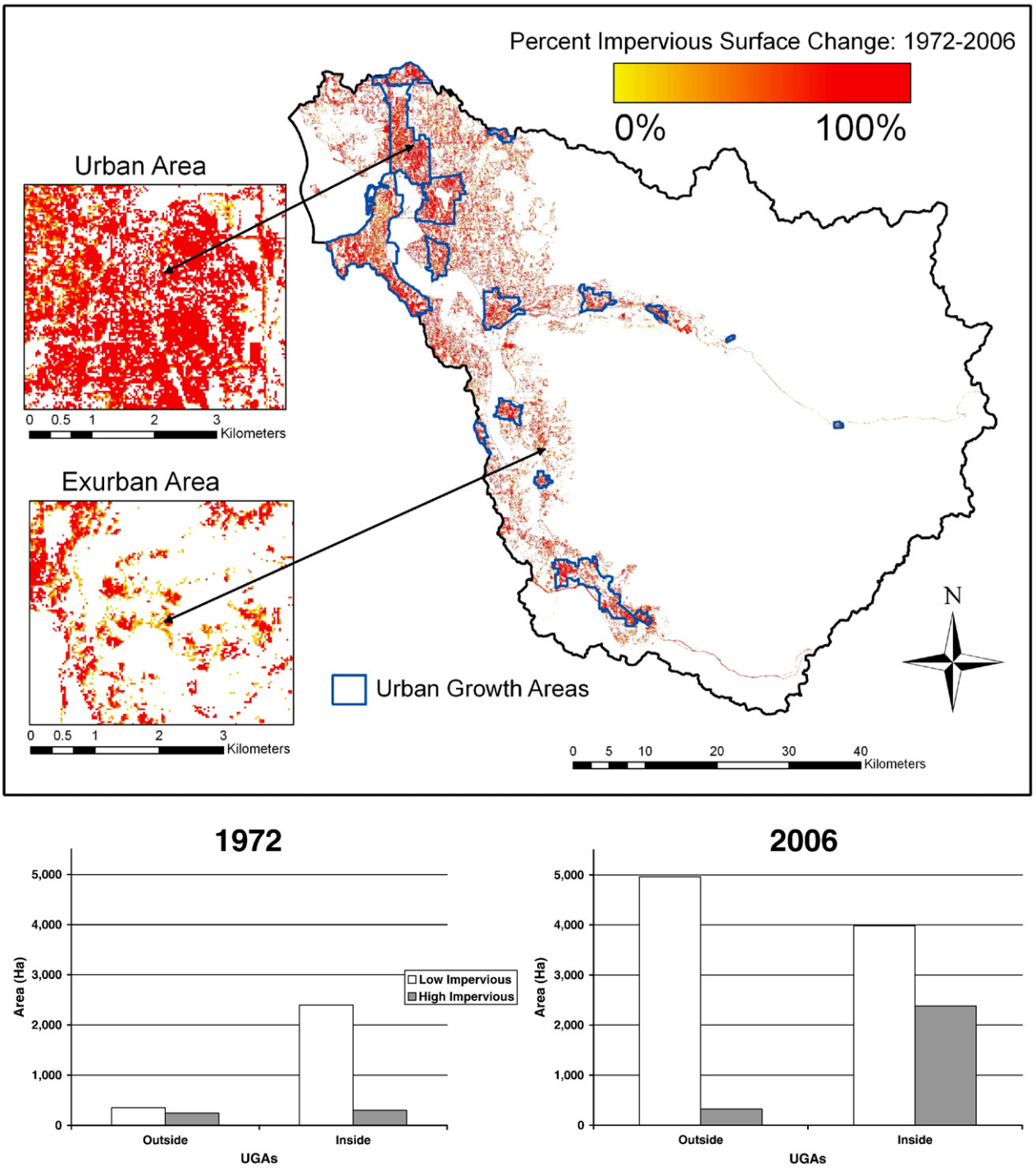

Fig. 8. Percent impervious surface change between 1972 and 2006 in the Snohomish WRIA. The bar charts depict the change in the area of low v. high impervious surface inside and outside the UGAs between 1972 and 2006.

(Fig. 9a). The NLCD map tended to represent these areas more uniformly, and therefore likely overestimated the amount of impervious surface. This was potentially due to the fact that like us, the NLCD mapping effort utilized an urban boundary mask to delineate areas with a high probability of impervious surface. However, we then used temporal rules to minimize commission error of impervious surface. In contrast to urban areas, in exurban areas, our map estimated a greater amount of impervious surface relative to the NLCD map (Fig. 9b). Across the entire study area, on a pixel level where either one or both studies mapped impervious surface, there was 35% agreement over the presence of impervious surface. More often, however, there was disagreement between the two maps. The NLCD mapped impervious surface (where we did not) 40% of the time, and we mapped impervious surface (where NLCD did not) 25% of the time (Fig. 9).

Alberti et al. (2004) estimated change in impervious surface over an eight year time period for a portion of the Snohomish

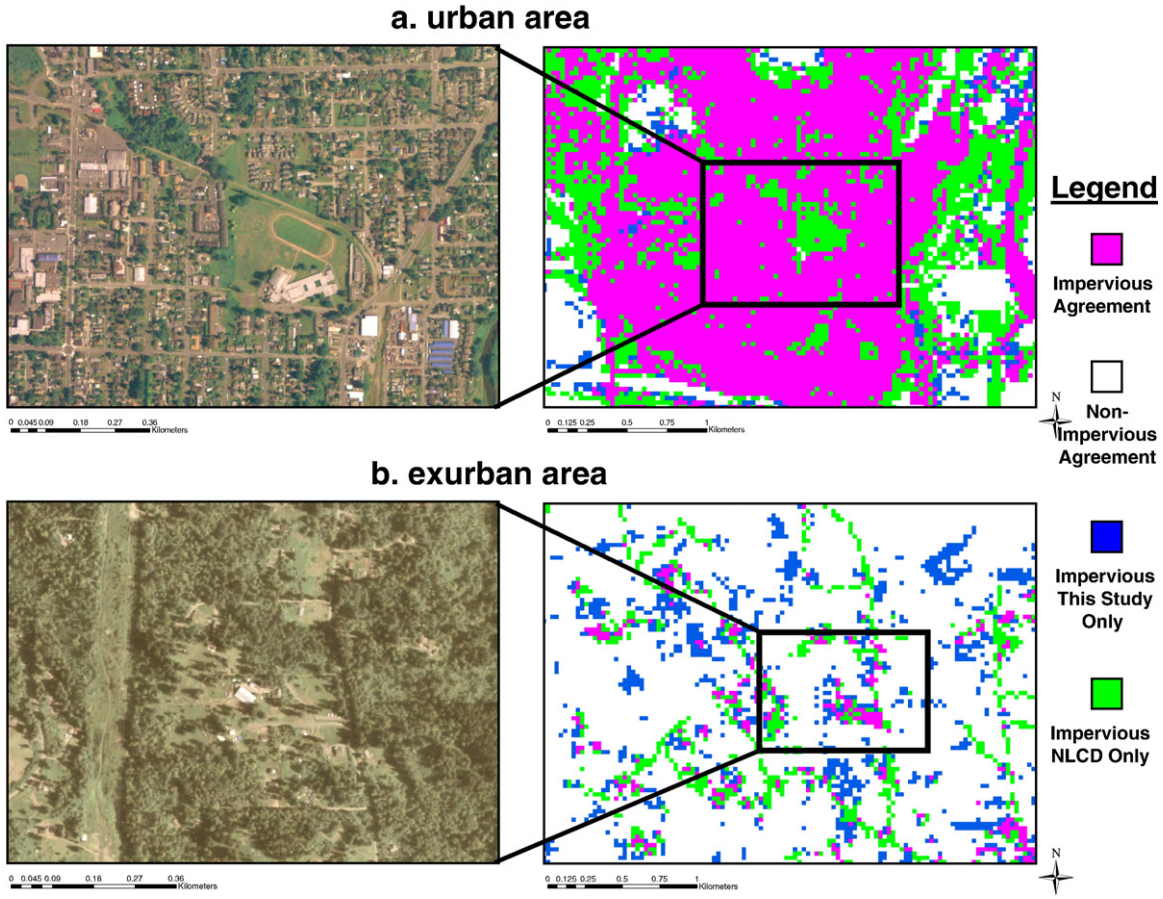

Fig. 9. Sample comparisons between NLCD 2001 impervious surface map and this study's 2002 impervious surface map. Top panel (a) is an example from an urban area; bottom panel (b) is an example from an exurban area. The thematic maps on the right depict agreement and disagreement between the NLCD 2001 map and our 2002 map. Magenta represents areas where both maps agree on impervious surface; white represents area where both maps agree on non-impervious surface; blue represents areas where only we map impervious surface; green represents areas where only NLCD maps impervious surface; Digital orthophoto is from 2005. (For interpretation of the references to colour in this figure legend, the reader is referred to the web version of this article.)

WRIA. Total impervious surface was estimated to increase by 9.7% between 1991 and 1999 across the study area. We compared these estimates to our maps for an eight year time period between 1990 and 1998. Our change detection indicated an increase of 15.2% in impervious surface across the study area over the eight years. One possible explanation for the divergence in change estimates was our inclusion of temporal rules. By examining the temporal trajectory of each pixel, we were able to discern real changes in impervious surface from false changes associated with vegetation phenology and succession. Moreover, our assumption that an impervious pixel could not revert back to non- or less-impervious was important. According to their change analysis, 11.6% of the paved class and 5.6% of the mixed urban class in 1991 reverted back to non-impervious in 1999. Our inclusion of temporal rules circumvented these types of illogical-change errors.

4. Conclusions

The use of a time series of Landsat imagery is an accurate and effective means of quantifying change in impervious surface across several decades for a large area. The 35 year Landsat archive is unique in this respect (Cohen & Goward, 2004), and lends itself to the development of multi-decadal time series for wide ranging applications, at local, regional, national, and international scales. Moderate resolution imagery, however, necessitates the use of a technique for sub-pixel unmixing, but this can only yield a preliminary land cover classification. To accurately identify impervious surface associated with urban and residential development requires the incorporation of spectral information into spatial and temporal information. We demonstrated that knowledge-based classification with spatial rules can help discriminate between otherwise spectrally indistinguishable land cover types. Furthermore, we demonstrated an effective technique to minimize classification error by examining the temporal trajectory of each pixel through the time series to identify non-impervious surfaces that were misclassified as impervious.

Comparisons to other studies provided compelling evidence that the inclusion of spatial and temporal rules were critical for mapping impervious surface. In the NLCD map, many non-impervious surfaces, especially in urban areas, were mapped as impervious surface. The most likely explanation for this was that open, non-vegetated surfaces were spectrally indistinguishable

from impervious surfaces. Therefore, spatial rules were necessary to distinguish open land cover from impervious surface. In addition, examining the temporal trajectory of each pixel yielded greater inference than could be gained from a single date alone, thereby minimizing classification error. Within urban areas, we reclassified pixels that were misclassified as impervious by incorporating temporal context.

Acknowledgements

Funding for this project was provided by the State of Washington Department of Fish and Wildlife and Governor's Salmon Recovery Office. The authors wish to thank Brian Cosentino of the Department of Fish and Wildlife and Stefan Coe of the Urban Ecology Research Lab at the University of Washington for their assistance assembling reference data. We also wish to thank three anonymous reviewers for their helpful comments.

References

Alberti, M., Weeks, R., & Coe, S. (2004). Urban land-cover change analysis in central Puget Sound. *Photogrammetric Engineering and Remote Sensing*, *70*(9), 1043−1052.

Arnold, C. L., Jr., & Gibbons, C. J. (1996). Impervious surface coverage: The emergence of a key urban environmental indicator. *Journal of the American Planning Association*, *62*(2), 243−258.

Barnes, K. B., Morgan, J. M., III, Roberge, M. C., & Lowe, S. (2007). *Sprawl development: its patterns, consequences, and measurement.* White paper available from http://chesapeake.towson.edu/landscape/urbansprawl/download/Sprawl_white_paper.pdf [accessed 15 March 2007].

Cadenasso, M. L., Pickett, S. T. A., & Schwarz, K. (2007). Spatial heterogeneity in urban ecosystems: Reconceptualizing land cover and a framework for classification. *Frontiers in Ecology and the Environment*, *5*(2), 80−88.

Canty, M. J., Nielsen, A. A., & Schmidt, M. (2004). Automatic radiometric normalization of multitemporal satellite imagery. *Remote Sensing of Environment*, *91*, 441−451.

Cohen, W. B., & Goward, S. N. (2004). Landsat's role in ecological applications of remote sensing. *BioScience*, *54*, 535−545.

Crist, E. P. (1985). A TM tasseled cap equivalent transformation for reflectance factor data. *Remote Sensing of Environment*, *17*, 301−306.

Crist, E. P., & Cicone, R. C. (1984). Application of the Tasseled Cap concept to simulated Thematic Mapper data. *Photogrammetric Engineering and Remote Sensing*, *50*, 343−352.

Dennison, P. E., & Roberts, D. A. (2003). Endmember selection for multiple endmember spectral mixture analysis using endmember average RMSE. *Remote Sensing of Environment*, *87*, 123−135.

Gong, P., & Howard, P. J. (1992). Land-use classification of SPOT HRV data using a cover-frequency method. *International Journal of Remote Sensing*, *13*(8), 1459−1471.

Guindon, B., Zhang, Y., & Dillabaugh, C. (2004). Landsat urban mapping based on a combined spectral-spatial methodology. *Remote Sensing of Environment*, *92*, 218−232.

Homer, C., Huang, C., Yang, L., & Wylie, B. (2002). Development of a circa 2000 land cover database for the United States. *Proceedings of the 2002 ASPRS Annual Convention, April 2002, Washington, D.C. CD-ROM.* Bethesda, MD: American Society for Photogrammetry and Remote Sensing.

Jensen, J. R. (1996). *Introductory Digital Image Processing: A Remote Sensing Perspective*, Second Edition. New Jersey: Prentice Hall.

Kauth, R. J., & Thomas, G. S. (1976). The Tasseled Cap — A graphic description of the spectral-temporal development of agricultural crops as seen by Landsat. *Proceedings, Symposium on Machine Processing of Remotely Sensed Data* (pp. 41−51). West Lafayette, IN: Laboratory for Applications of Remote Sensing.

Kennedy, R. E., & Cohen, W. B. (2003). Automated designation of tie-points for image-to-image coregistration. *International Journal of Remote Sensing*, *24* (17), 3467−3490.

King County GIS Center. (2007). *Current King County Urban Growth Area Boundaries.* Available from http://www5.metrokc.gov/sdc/Metadata.aspx?Layer=ugline04&XMLAvail=True [accessed 15 March 2007].

Liu, H., & Zhou, Q. (2004). Accuracy analysis of remote sensing change detection by rule-based rationality evaluation with post-classification comparison. *International Journal of Remote Sensing*, *25*(5), 1037−1050.

Lu, D., & Weng, Q. (2004). Spectral mixture analysis of the urban landscape in Indianapolis with Landsat ETM+ imagery. *Photogrammetric Engineering and Remote Sensing*, *70*, 1053−1062.

Lu, D., & Weng, Q. (2005). Urban classification using full spectral information of Landsat ETM+ Imagery in Marion County, Indiana. *Photogrammetric Engineering and Remote Sensing*, *71*(11), 1275−1284.

Lu, D., & Weng, Q. (2006). Use of impervious surface in urban land-use classification. *Remote Sensing of Environment*, *102*, 146−160.

Masek, J. G., Vermote, E. F., Saleous, N., Wolfe, R., Hall, E. F., Huemmrich, F., et al. (2006). A Landsat surface reflectance data set for North America, 1990–2000. *Geoscience and Remote Sensing Letter*, *3*, 68−72.

Phinn, S., Stanford, M., Scarth, P., Murray, A. T., & Shyy, P. T. (2002). Monitoring the composition of urban environments based on the vegetation-impervious surface-soil (VIS) model by subpixel analysis techniques. *International Journal of Remote Sensing*, *23*, 4131−4153.

Radeloff, V. C., Hammer, R. B., & Stewart, S. I. (2005). Rural and suburban sprawl in the U.S. Midwest from 1940 to 2000 and its relation to forest fragmentation. *Conservation Biology*, *19*(3), 793−805.

Rashed, T., Weeks, J. R., Roberts, D., Rogan, J., & Powell, R. (2003). Measuring the physical composition of urban morphology using multiple endmember spectral mixture models. *Photogrammetric Engineering and Remote Sensing*, *69*, 1011−1020.

Ridd, M. K. (1995). Exploring a V–I–S (vegetation–impervious surface–soil) model for urban ecosystem analysis through remote sensing: comparative anatomy for cities. *International Journal of Remote Sensing*, *16*, 2165−2185.

Schroeder, T. A., Cohen, W. B., Song, C., Canty, M. J., & Yang, Z. (2006). Radiometric correction of multi-temporal Landsat data for characterization of early successional forest patterns in western Oregon. *Remote Sensing of Environment*, *103*, 16−26.

Small, C. (2002). Multitemporal analysis of urban reflectance. *Remote Sensing of Environment*, *81*, 427−442.

Small, C. (2003). High spatial resolution spectral mixture analysis of urban reflectance. *Remote Sensing of Environment*, *88*, 170−186.

Snohomish County Cartography/GIS Services Team. (2007). *Urban Growth Areas.* Available from ftp://ftp.co.snohomish.wa.us/Planning & Devel Services/Urban Growth Areas/ugabdy_polygon.shp [accessed 15 March 2007].

Tang, Z. X., Engel, B. A., Lim, K. J., Pijanowski, B. C., & Harbor, J. (2005). Minimizing the impact of urbanization on long term runoff. *Journal of the American Water Resources Association*, *41*(6), 1347−1359.

United States Environmental Protection Agency. (2007). *Multi-Resolution Land Characteristics Consortium, National Land Cover Database, 2001.* Available from http://www.epa.gov/mrlc/nlcd.html [accessed 15 March 2007].

Washington Office of Financial Management. (2007). *Historical/Current Data Set: Total Resident Population by Year by County, Washington, 1960 to 2006.* Available from http://www.ofm.wa.gov/pop/coseries/ [accessed 19 March 2007].

Washington State Department of Natural Resources. (2007). *Washington State Waterbodies Hydrography.* Available from http://www3.wadnr.gov/dnrapp6/dataweb/dmmatrix.html [accessed 15 March 2007].

Washington State Department of Transportation. (2007). *State Highways, at 24 k.* Available from http://www.wsdot.wa.gov/mapsdata/GeoDataCatalog/default.htm [accessed 15 March 2007].

Wu, C. (2004). Normalized spectral mixture analysis for monitoring urban composition using ETM+ imagery. *Remote Sensing of Environment*, *93*, 480−492.

Wu, C., & Murray, A. T. (2003). Estimating impervious surface distribution by spectral mixture analysis. *Remote Sensing of Environment*, *84*, 493−505.

Xian, G., & Crane, M. (2005). Assessments of urban growth in the Tampa Bay watershed using remote sensing data. *Remote Sensing of Environment*, *97*, 203−215.

Yang, L., Huang, C., Homer, C. G., Wylie, B. K., & Coan, M. J. (2003). An approach for mapping large-area impervious surfaces: synergistic use of Landsat-7 ETM+ and high spatial resolution imagery. *Canadian Journal of Remote Sensing*, *29*(2), 230−240.

Yang, L., Xian, G., Klaver, J. M., & Deal, B. (2003). Urban land-cover change detection through sub-pixel imperviousness mapping using remotely sensed data. *Photogrammetric Engineering and Remote Sensing*, *69*(9), 1003−1010.

Yang, X. (2002). Satellite monitoring of urban spatial growth in the Atlanta metropolitan area. *Photogrammetric Engineering and Remote Sensing*, *68*(7), 725−734.

Yuan, F., Sawaya, K. E., Loeffelholz, B. C., & Bauer, M. E. (2005). Land cover classification and change analysis of the Twin Cities (Minnesota) metropolitan area by multitemporal Landsat remote sensing. *Remote Sensing of Environment*, *98*, 317−328.